OPTICA

Miniaturized computational spectrometer based on two-photon absorption

Yaotian Zhao,[1,†] Xuhan Guo,[1,4,†] Jinlong Xiang,[1] Zhenyu Zhao,[1] Yujia Zhang,[1] Xi Xiao,[2,5] Jia Liu,[3] Daigao Chen,[3] and Yikai Su[1]

[1]State Key Laboratory of Advanced Optical Communication Systems and Networks, Department of Electronic Engineering, Shanghai Jiao Tong University, Shanghai 200240, China
[2]State Key Laboratory of Optical Communication Technologies and Networks, China Information and Communication Technologies Group Corporation (CICT), Wuhan 430074, China
[3]National Optoelectronics Innovation Center, Wuhan 430074, Hubei, China
[4]guoxuhan@sjtu.edu.cn
[5]xiaoxi@noeic.com
[†]These authors contributed equally to this work.

Received 7 December 2023; revised 4 February 2024; accepted 16 February 2024; published 15 March 2024

On-chip spectrometers hold significant promise in the development of laboratory-on-a-chip applications. However, the spectrometers usually require extra on-chip or off-chip photodetectors (PDs) to sense optical signals, resulting in increased footprints and costs. In this paper, we address this issue by proposing a fully on-chip spectrometer based on two-photon absorption (TPA) in a simple micro-ring resonator (MRR) configuration. While TPA is a commonly undesired phenomenon in conventional silicon devices due to its attached absorption losses and nonlinearity, we exploit it as a powerful and efficient tool for encoding spectral information, instead of using additional PDs. The input spectrum can be reconstructed from the sensed TPA current. Our proposed spectrometer achieves a bandwidth of 10 nm with a resolution of 0.4 nm while occupying a small footprint of only 16 × 16 μm^2, and the bandwidth can be further improved through several cascaded MRRs. This advancement could enable forward fully integrated and miniaturized spectrometers with low cost, which holds far-reaching applications in *in situ* biochemical analysis, remote sensing, and intelligent healthcare.

https://doi.org/10.1364/OPTICA.511658

Spectrometers have wide applications in sensing and monitoring [1–3]. Integrated spectrometers are especially attractive because they can be manufactured with low cost and small footprint, which may boost the development of laboratory-on-a-chip applications [4–6]. Among various approaches to miniaturized spectrometers, silicon photonics is the most promising due to its compatibility with large-scale CMOS manufacturing technology with various available functional components.

Numerous approaches have been carried out to realize high-performance silicon spectrometers, which fall broadly into four categories [7]. First, some spectrometers employ dispersive optics, such as planar photonic crystals [8,9], planar echelle gratings [10], arrayed waveguide gratings [11,12], etc., to split light toward spatially separated photodetectors (PDs). Although this approach theoretically operates with a broad spectral bandwidth and a high resolution, the miniaturization usually necessitates a compromise in performance, as the resolution is inherently tied to the optical path length afforded by the footprint. Second, some spectrometers use narrowband filters like micro-ring resonators (MRRs) [13–15] and nanobeams [16] to route different spectral components to different PDs. While these narrowband filters offer smaller footprints than those based on dispersive systems, they still require a large number of filters and PDs. Thirdly, Fourier transform microspectrometers based on a Mach–Zehnder-interferometer (MZI) structure have also been realized on a silicon photonics platform [17–19]. Heaters are integrated between the two MZI arms to change the phase delay. This kind of spectrometer can benefit from an improved signal-to-noise ratio (SNR). However, there are some challenges such as high power consumption, a large driving voltage, long measurement times, and a large footprint.

Recently, a fourth paradigm in spectrometry has emerged, known as the "reconstructive" or "computational" spectrometer. These spectrometers feature a set of PDs encoded with distinctive spectral response characteristics. By measuring the PDs in parallel and leveraging some advanced algorithms, the sensed signals can reconstruct the incident light spectrum. The reconstructive spectrometers are implemented in either a static or dynamic scenario. In the static approach, the optical power is divided into different channels, and each channel routes the power to different PDs. Several structures have been developed in this scenario, including stratified waveguide filters [20], random photonic crystals [21–23], multimode spiral waveguides [24,25], etc. This method provides a robust and fast multi-channel detection but suffers from larger device footprints and compromise in the received power at each channel. On the other hand, the dynamic approach has a more compact footprint by employing a tunable device such as tunable nanobeams [26], MRRs [27], micro-disks [28], MZIs [29], metasurfaces [30], etc. The detected power is considered as different channels when the device works at different temperatures. This method can greatly reduce the device footprint

without largely compromising performance. However, it may pose a challenge to ensure stable and repeatable working conditions, which are crucial for accurate spectral characterization. Overall, various high-performance spectrometers have been successfully integrated on a silicon platform; however, all the aforementioned devices require extra on-chip or off-chip PDs, which require larger footprints and costs. The miniaturization of spectrometers with low cost still holds considerable potential, and the fully integrated ultra-compact spectrometer is still highly desired for high-density photonic integrated circuits.

Here, we propose a novel approach utilizing a single MRR assisted with two-photon absorption (TPA) effects to fully perform the functions of a spectrometer without external photodetectors. Although TPA is usually unwanted in conventional MRR due to the attached absorption losses and its nonlinearity, this drawback can become a treasure by encoding the spectral information in it. By measuring the TPA current at different temperatures through a micro-heater, the incident spectrum can be reconstructed in a computational approach. The proposed device achieves a bandwidth of 10 nm and a resolution of 0.4 nm, all within an ultracompact footprint of $16 \times 16\ \mu m^2$. The proposed approach may contribute to the advancement of fully integrated, high-performance spectrometers on a silicon photonics platform, offering a powerful tool for photonic integrated circuit applications.

The principle of the proposed computational spectrometer is illustrated in Fig. 1. During the TPA process, two photons can be simultaneously absorbed to generate free carriers. To sense the TPA signals, we make the TPA processes happen in the depletion region of a reverse biased PN junction, and then the generated free carriers are sensed from the current signals. The cross-section view of the MRR is shown in Fig. 1(b). The MRR is designed to operate in an all-pass configuration and is doped to create a PN junction. Two electrodes are contacted to the doping area and provide a reverse voltage bias to sense the TPA current. A micro-heater is also included on the top of the ring to tune the working temperature. Two other electrodes are contacted to the heater on another metal layer. When the light resonates in the MRR, more free carriers are generated from the TPA effect, and the current responses in the reverse PN junction can be measured by a source meter. The nonlinear micro-ring model allows us to determine the relationship between the optical power spectrum and the photocurrent generated by TPA (see details in Section 1 of Supplement 1).

Figure 1(c) shows the computational processes to reconstruct the input spectrum. The detected current I_{ph} of an unknown signal with spectrum power $S(\lambda)$ can be mathematically written as Eq. (1) [31]:

$$I_{ph} = \int \gamma(\lambda)\, S^2(\lambda)\, d\lambda. \tag{1}$$

The MRRs working at different temperatures serve as different sensing channels. This formulation provides N linear algebraic equations to determine M unknown values of the input signal, $S^2(\lambda)$, which can be discretized as Eq. (2):

$$I_{ph,N\times 1} = \gamma_{N\times M}\, S^2_{M\times 1}. \tag{2}$$

The sampling matrix $\gamma_{N\times M}$ is obtained through a calibration, and the TPA current $I_{ph,N\times 1}$ is obtained by direct measurement. Then the target spectrum $S^2_{M\times 1}$ is calculated by solving the matrix. A linear regression algorithm is utilized to help to solve the matrix by minimizing l_2 norm as Eq. (3):

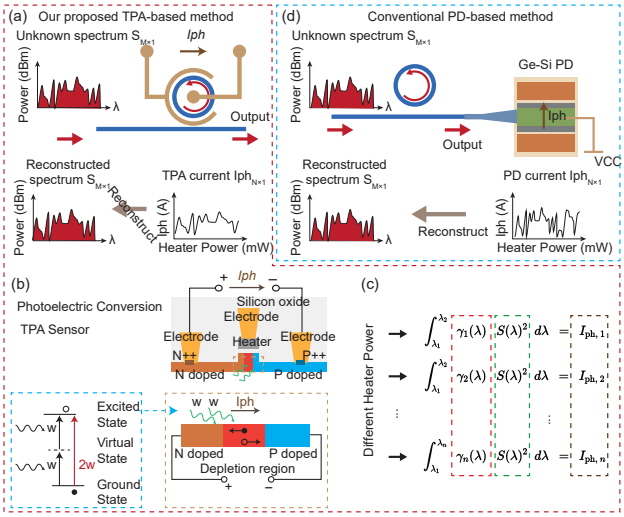

Fig. 1. (a) Schematic of the spectrometer based on micro-ring resonator (MRR); the two-photon absorption (TPA) current is employed to reconstruct the unknown input spectrum. (b) Cross-section of the PN junction rib waveguide on a silicon-on-insulator (SOI) substrate, which is used to sense the TPA current. (c) Principles behind computational spectrometers based on TPA responses that encode spectral response characteristics. (d) Conventional spectrometers based on photodetectors (PDs).

$$\text{minimize}||I - \gamma S^2||^2. \tag{3}$$

For the case with stronger measurement noise, regularization of the l_2 norm of S can be added to the regression with a certain weight coefficient α for smooth spectrum reconstruction as Eq. (4) [20]:

$$\text{minimize}\ ||I - \gamma S^2||^2 + \alpha||S^2||^2. \tag{4}$$

TPA spectrometer characterization. The proposed MRR is fabricated in a commercial 8-inch 130 nm CMOS foundry. The MRR is based on a 220 nm silicon-on-insulator (SOI) platform. The radius of the MRR is 8 μm. The waveguide width is 420 nm, and the slab thickness is 70 nm. To maintain the MRR working near the critical coupling region, the racetrack is 5 μm with a gap width of 280 nm. The doping concentration is $3 \times 10^{18}\ cm^{-3}$ for both P- and N-type doping. A lateral PN junction working with depletion mode is placed in the MRR with the widths for P-type doping of 230 nm and N-type doping of 190 nm. Figure 2(a) is the microscope picture of the fabricated MRR. The metal pads are designed with a pitch of 150 μm, which is further packaged through wire bonding.

Figure 2(b) shows the experimental setup to measure the optical properties and TPA current responses of the fabricated MRR. The light is generated from a tunable semiconductor laser (TSL, Santec TSL-770), then the polarization is tuned through a fiber polarization controller (PC). The light is coupled into the MRR through grating couplers. An off-chip photodetector (Santec MPM-210) is employed for optical alignment and receiving the transmitted power. Here, one source meter (SM1, Keithley 2400) is employed to control the heater voltage bias, and another source meter (SM2, Keithley 2400) is used to measure the TPA current.

To address the superior performance of the TPA spectrometer, we use the PD as the monitor and reference. Figure 2(c) shows the PD received optical power and TPA current responses. Specifically,

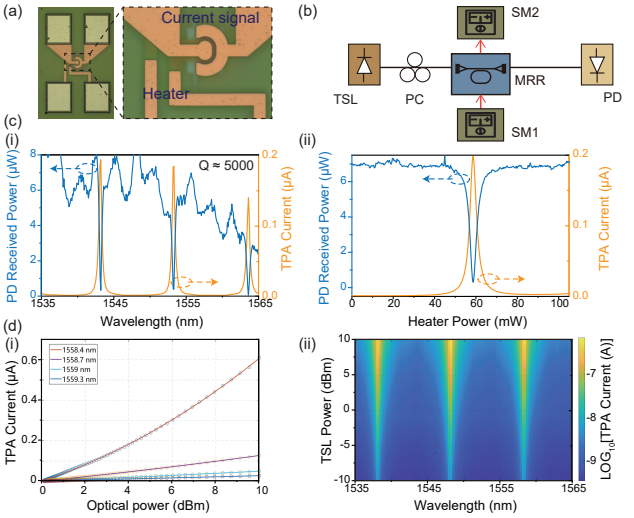

Fig. 2. (a) Optical microscope photos of the fabricated micro-ring resonator (MRR). (b) Experimental setup to measure the MRR's prosperities. (c) PD received power and two-photon absorption (TPA) current responses at different wavelengths and heater powers. (d) Measured TPA current with different input optical powers.

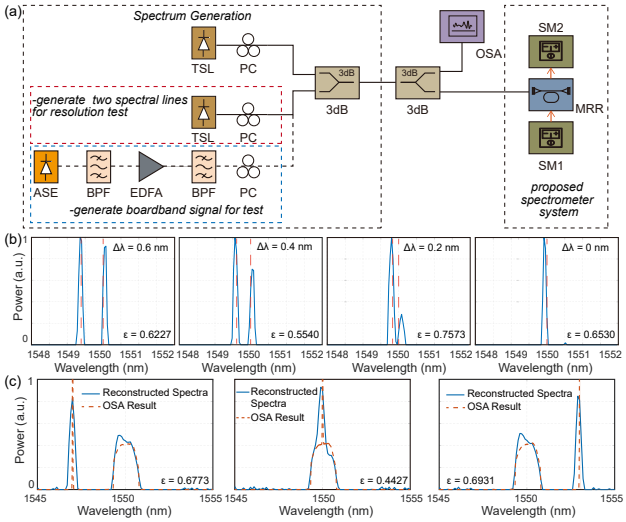

Fig. 3. (a) Experimental setup to estimate the spectrometer's performance. (b) Reconstructed spectra with different wavelength spacings. (c) Reconstructed broadband spectra with the narrow peak signals at different locations.

Fig. 2(c-i) shows the PD received power and the sensed TPA current when the input wavelength changes. The Q factor of the MRR is around 5000 with a full width at half maximum (FWHM) around 0.3 nm. Besides, when the light resonates in the MRR, it generates more free carries, leading to a larger TPA current. The FWHM of the TPA current response is around 0.2 nm. Compared to the PD-measured result, the TPA current has a smaller FWHM because the TPA current evolves with the square of the optical power. The narrower FWHM can benefit a higher resolution of the spectrometer. Figure 2(c-ii) shows the thermo-optic properties of the proposed MRR. The resonant wavelength moves towards the input wavelength of 1550 nm, causing the dip of the curve. The change of resonant wavelength will also cause a rise in the TPA current response as shown by the yellow line. To verify the relationship between the optical power and TPA current, Fig. 2(d) shows the measured TPA current responses with different input optical powers. In Fig. 2(d-i), the scatter points show the TPA current responses at different wavelengths, and the solid lines show the fitted results. The measured TPA current is not exactly the square of the input power, which may be attributed to the avalanche amplification and saturation of the free carriers in the PN junction. Figure 2(d-ii) plots the TPA current responses with different input optical power and wavelength simultaneously, which indicates this relationship is suitable for all conditions. The detailed information of the TPA sensor is shown in Supplement 1.

For the pre-equalization of the nonlinearity, since the TPA process is a third-order nonlinear effect, the relationship between the photocurrent (I_{ph}) and optical power at wavelength λ is expressed as $I_{ph} = \gamma P^{\mu}(\lambda)$ [13], where $\mu \approx 2$ indicates the power-law nature; the coefficient γ is linked to TPA coefficients $\beta_{\mathrm{TPA}}(\lambda)$, losses from the MRR, grating, and other components. Notably, $\gamma(\lambda)$ is obtained through a calibration process, leveraging a known spectrum as the input with a tunable laser source [see details in Section 6 of Supplement 1].

To characterize the performance of the TPA spectrometer, various types of optical signals are demonstrated as the input and reconstructed by the approach mentioned above. The actual resolution of the proposed spectrometer system is determined by the ability to distinguish two closely spaced spectral lines. Figure 3(a) shows the experimental setup to estimate the resolution. The two TSLs are used to generate a target spectrum S that has two closely spaced spectral lines. More information of the sampling matrix γ is shown in Section 2 of Supplement 1. In the measurement process, the TPA current matrix I_{ph} is obtained from SM2 when we sweep the SM1 voltages. The spectrum S is reconstructed from the TPA current matrix via nonlinear minimization as Eq. (4) with a MATLAB toolbox named CVX [32]. The reconstructed spectrum is shown in Fig. 3(b). The dashed lines show the input spectrum with two known separate spectral lines, while the solid lines show the reconstructed spectrum. The two separate reconstructed spectral lines are gradually unable to be distinguished as the decrease of wavelength space, which indicates the actual resolution of the proposed spectrometer system is about 0.4 nm approximately.

Figure 3 also shows the broadband signal response of the fabricated MRR spectrometer. A broadband spectrum is generated from an amplified spontaneous emission (ASE) source. An optical spectrum analyzer (OSA) is employed to measure the output spectrum as a reference. As discussed, the sensed TPA current signal from SM2 can reconstruct the input spectrum. The reconstructed spectra with different TSL wavelengths are shown as solid lines in Fig. 3(c). The dashed line shows the measured result from the OSA as a reference. The proposed spectrometer system has shown a bandwidth of 10 nm. The measured result largely agrees with the OSA measured result. The slight misalignment between the reconstructed spectral lines and input spectral lines is attributed to the environmental variation in the calibration and measurement processes, resulting from temperature changes and mechanical vibrations of the fiber. The results can be further improved by the temperature controller and optical package. To evaluate the accuracy of the reconstruction, we introduce the parameter ε, defined as $\varepsilon = \frac{||S_0 - S||_2}{||S_0||_2}$, where S is the reconstructed spectrum, and S_0 is the reference spectrum [29].

Leveraging the TPA features of the silicon, the proposed computational TPA spectrometer can realize a complete on-chip spectrum analysis. Figure 4 shows a comparison of the reported integrated reconstructive micro-spectrometers in the past few

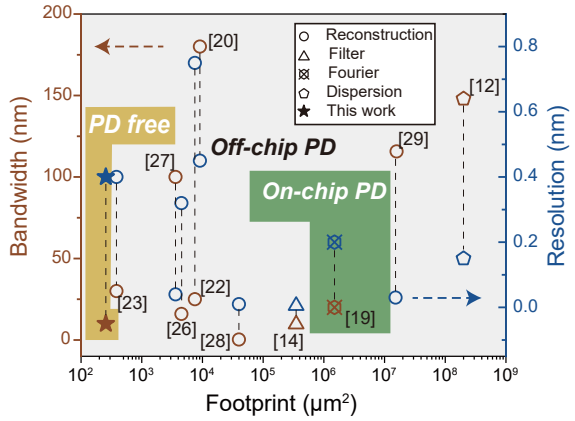

Fig. 4. Comparison of the state-of-the-art silicon spectrometer.

years. Here, the footprint only takes into account the passive components without PDs. Compared to the reconstructive spectrometers that use PDs as the photoelectric converter for spectrum detection, our proposed TPA-based spectrometer not only gets rid of extra PDs, but also has a record compact size. A detailed comparison table is also provided in Section 4 of Supplement 1. Besides, the current response of TPA could be shaper than that from PDs, as it evolves as the square of the optical power. A sharper current response will lead to a better resolution for the same design. However, this work also has some limitations and needs further improvements. The TPA current is much smaller than the PD current, which may lead to a worse responsiveness. The input power should exceed −10 dBm in current design. Besides, the MRR was previously in order to construct a modulator [33]; thus, its structure is not fully optimal for a spectrometer design that requires a narrow FWHM, which causes a limited resolution. The limited FSR of MRR is also responsible for the limited bandwidth of the spectrometer, which can be improved to 30 nm by cascaded MRRs or other designs as shown in Section 5 of Supplement 1.

In this study, we report a fully on-chip spectrometer with a record compact footprint of 16 × 16 μm^2. The target spectrum is reconstructed from the TPA current responses that encode the light spectrum. The proposed tunable MRR can reconstruct the input spectra with a resolution of 0.4 nm and a bandwidth of 10 nm and can be further improved to 30 nm through several cascaded MRRs. The proposed approach can realize an ultra-compact spectrometer and get rid of external PDs. The bandwidth and resolution of the spectrometer still have considerable potential improvements by cascading MRR with a higher quality factor. A viable route for enhancing the proposed method is also proposed in Section 9 of Supplement 1. Such an ultra-compact and fully integrated spectrometer is highly desired for on-chip optical sensing, which is expected to boost the development of lab-on-a-chip systems significantly.

Funding. National Key Research and Development Program of China (2021YFB2801903); National Natural Science Foundation of China (61835008, 62175151); Shanghai Municipal Science and Technology Major Project.

Acknowledgment. We thank the Center for Advanced Electronic Materials and Devices (AEMD) of Shanghai Jiao Tong University (SJTU) for their support in device fabrication.

Disclosures. The authors declare no conflicts of interest.

Data availability. Data are available upon reasonable request.

Supplemental document. See Supplement 1 for supporting content.

REFERENCES

1. W. R. Brode, *Chemical Spectroscopy* (Wiley, 1939).
2. K. B. Beć, J. Grabska, and C. W. Huck, Molecules **25**, 2948 (2020).
3. A. J. Simpson, D. J. McNally, and M. J. Simpson, Prog. Nucl. Magn. Resonan. Spectrosc. **58**, 97 (2011).
4. D.-X. Xu, J. H. Schmid, G. T. Reed, *et al.*, IEEE J. Sel. Top. Quantum Electron. **20**, 189 (2014).
5. H. Lin, Z. Luo, T. Gu, *et al.*, Nanophotonics **7**, 393 (2017).
6. A. J. McGonigle, T. C. Wilkes, T. D. Pering, *et al.*, Sensors **18**, 223 (2018).
7. Z. Yang, T. Albrow-Owen, W. Cai, *et al.*, Science **371**, eabe0722 (2021).
8. B. Gao, Z. Shi, and R. W. Boyd, Opt. Express **23**, 6491 (2015).
9. B. Momeni, E. S. Hosseini, and A. Adibi, Opt. Express **17**, 17060 (2009).
10. R. Cheng, C.-L. Zou, X. Guo, *et al.*, Nat. Commun. **10**, 4104 (2019).
11. P. Cheben, J. H. Schmid, A. Delâge, *et al.*, Opt. Express **15**, 2299 (2007).
12. G. Calafiore, A. Koshelev, S. Dhuey, *et al.*, Light Sci. Appl. **3**, e203 (2014).
13. A. Nitkowski, L. Chen, and M. Lipson, Opt. Express **16**, 11930 (2008).
14. L. Zhang, M. Zhang, T. Chen, *et al.*, Opto-Electron. Adv. **5**, 210100 (2022).
15. Z. Zhang, Y. Wang, and H. K. Tsang, ACS Photon. **8**, 1251 (2020).
16. P. Deotare, L. Kogos, Q. Quan, *et al.*, in *Conference on Lasers and Electro-Optics (CLEO)* (IEEE, 2012), pp. 1–2.
17. M. C. Souza, A. Grieco, N. C. Frateschi, *et al.*, Nat. Commun. **9**, 665 (2018).
18. A. Li, J. Davis, A. Grieco, *et al.*, Photon. Res. **8**, 219 (2020).
19. D. M. Kita, B. Miranda, D. Favela, *et al.*, Nat. Commun. **9**, 4405 (2018).
20. A. Li and Y. Fainman, Nat. Commun. **12**, 2704 (2021).
21. W. Hartmann, P. Varytis, H. Gehring, *et al.*, Nano Lett. **20**, 2625 (2020).
22. B. Redding, S. F. Liew, R. Sarma, *et al.*, Nat. Photonics **7**, 746 (2013).
23. W. Hadibrata, H. Noh, H. Wei, *et al.*, Laser Photon. Rev. **15**, 2000556 (2021).
24. B. Redding, S. Fatt Liew, Y. Bromberg, *et al.*, Optica **3**, 956 (2016).
25. E. Edrei, N. Cohen, E. Gerstel, *et al.*, Sci. Adv. **8**, eabn3391 (2022).
26. J. Zhang, Z. Cheng, J. Dong, *et al.*, Optica **9**, 517 (2022).
27. H. Xu, Y. Qin, G. Hu, *et al.*, Light Sci. Appl. **12**, 64 (2023).
28. C. Sun, Z. Chen, Y. Ye, *et al.*, Laser Photon. Rev. **17**, 2200792 (2023).
29. C. Yao, M. Chen, T. Yan, *et al.*, Light Sci. Appl. **12**, 156 (2023).
30. J. Xiong, X. Cai, K. Cui, *et al.*, "Dynamic brain spectrum acquired by a real-time ultra-spectral imaging chip with reconfigurable metasurfaces," arXiv, arXiv:2005.02689 (2020).
31. Y. Ren and V. Van, IEEE J. Sel. Top. Quantum Electron. **26**, 1 (2020).
32. M. Grant, S. Boyd, and Y. Ye, *CVX: Matlab Software for Disciplined Convex Programming* (CVX Research, 2008).
33. Y. Zhang, H. Zhang, J. Zhang, *et al.*, Photon. Res. **10**, 1127 (2022).